Society of Medical Education & Research

2025, Volume 5, Issue 1, Page No: 43-56
ISSN: 3108-4826

Journal of Medical Sciences and Interdisciplinary Research

Histological Validation and Clinical Application of 3D MR Fingerprinting-Derived Myelin Water Fraction in Brain Development and Leukodystrophy

Wei Jian Zhang[1]*, Liang Chen[1], Hao Ming Zhou[2], Qiang Sun[2], Bo Liu[3], Yifan Wang[3]

[1]School of Management, Fudan University, Shanghai, China.
[2]School of Business Administration, Shanghai Jiao Tong University, Shanghai, China.
[3]School of Economics and Management, Tongji University, Shanghai, China.

***E-mail** ✉ w.zhang.fudan@outlook.com

Abstract

Magnetic resonance fingerprinting (MRF) allows rapid, noninvasive estimation of myelin content through the myelin water fraction (MWF), providing a tool for monitoring brain maturation and pathological changes. Despite this potential, MRF-derived MWF has not been systematically validated against histology, and its application in leukodystrophy remains unexplored. The present study aimed to confirm the histological basis of MRF-derived MWF in mice and to investigate how MWF relates to myelin, developmental stage, and leukodystrophy in both murine models and pediatric populations, demonstrating its translational potential. We performed 3D MRF on normal C57BL/6 mice at multiple ages, on megalencephalic leukoencephalopathy with subcortical cyst 1 wild type (MLC1 WT) mice, and on MLC1 knock-out (MLC1 KO) mice using a 3 T MRI system. MWF maps were extracted from the 3D MRF datasets, and myelin content was quantified histologically using anti-proteolipid protein (PLP) staining in the corpus callosum and cortex. Relationships between 'MWF and PLP' and between 'MWF and age' were evaluated in C57BL/6 mice. Differences in MWF were compared between MLC1 WT and KO mice. Retrospective data from 81 normally developing children were analyzed to assess age-dependent changes in MWF. In 35 C57BL/6 mice (ages 3–48 weeks), MWF showed significant positive associations with PLP immunoreactivity in both the corpus callosum ($\beta = 0.0006$, $P = 0.04$) and cortex ($\beta = 0.0005$, $P = 0.006$). In 12-week-old C57BL/6 mice, MWF correlated strongly with PLP ($\beta = 0.0009$, $P = 0.003$, $R^2 = 0.54$). Age-dependent increases in MWF were observed in the corpus callosum ($\beta = 0.0022$, $P < 0.001$) and cortex ($\beta = 0.0010$, $P < 0.001$). Seven MLC1 WT and nine MLC1 KO mice displayed significantly different MWF values in both regions ($P < 0.001$ for corpus callosum and cortex). In 81 children (median age 126 months, range 0–199 months), MWF changes with age were best described by a third-order polynomial regression (adjusted $R^2 = 0.44$–0.94, $P < 0.001$). MWF closely reflected histologically measured myelin, age-related maturation, and the presence of leukodystrophy, supporting 3D MRF-derived MWF as a rapid, noninvasive quantitative marker of myelin in both animal models and humans.

Keywords: Magnetic resonance fingerprinting, Myelin water fraction, Proteolipid protein, Brain, Development, Children

Introduction

MRF is a quantitative imaging approach suitable for evaluating brain development [1, 2], allowing simultaneous acquisition of T1 and T2 relaxation times in a single, time-efficient scan [3]. These relaxation parameters reflect tissue composition changes that occur during maturation [1]. In addition to T1 and T2, MRF can quantify myelin by distinguishing myelin-associated water from free or intra/extracellular water using relaxation time characteristics [4]. The myelin water fraction (MWF) is defined as the proportion of myelin-associated water relative to total tissue water [1, 5].

MWF serves as a developmental marker because myelination is tightly coupled to neural growth [6, 7].

Access this article online https://smerpub.com/

Received: 15 November 2024; **Accepted:** 18 February 2025

How to cite this article: Zhang WJ, Chen L, Zhou HM, Sun Q, Liu B, Wang Y. Histological Validation and Clinical Application of 3D MR Fingerprinting-Derived Myelin Water Fraction in Brain Development and Leukodystrophy. J Med Sci Interdiscip Res. 2025;5(1):43-56. https://doi.org/10.51847/RaQVGlUyfR

While traditional T1- and T2-weighted imaging provides qualitative myelination assessment [8], quantitative metrics including diffusion tensor imaging, relaxation times, and MWF offer more precise evaluation [1, 6, 9]. Prior studies have measured T1, T2, and MWF using 2D MRF in 28 children aged 0–5 years [1], and 3D MRF-derived T1/T2 relaxation times in 25 neonates (median corrected gestational age 263 days) [2]. However, histological validation of 3D MRF-derived MWF is lacking.

Inherited white matter disorders affect approximately 1 in 8,000 births [10]. Brain MRI is a crucial tool for detecting pediatric WM diseases [9, 11], yet few studies have applied MRF-derived MWF to leukodystrophies. Megalencephalic leukoencephalopathy with subcortical cysts (MLC) is an autosomal recessive disorder characterized by early-onset cerebral WM edema and myelin vacuolation [12, 13]. Patients develop macrocephaly during infancy, with clinical stabilization thereafter [13]. MRI shows diffuse WM swelling and increased water content [13, 14], while histology reveals fluid-filled vacuoles in myelin sheaths [15], potentially affecting MWF measurements in specific regions [16]. Because studies validating 3D MRF-derived MWF histologically and in leukodystrophy are lacking, we aimed to examine MWF-histology correlations and age effects in mice. Furthermore, we analyzed

Materials and Methods

Animal study

Mice

All procedures involving animals adhered to guidelines from the National Institutes of Health and the Institutional Animal Care and Use Committee at The Catholic University of Korea. To investigate myelination patterns during brain maturation, 35 C57BL/6 mice (19 females) underwent scanning between October 2021 and March 2022, spanning ages from 3 to 48 weeks. For assessing myelination in a leukodystrophy context, 9 MLC1 wild-type (WT, serving as controls) and 9 MLC1 knock-out (KO, modeling leukodystrophy) mice were imaged from December 2021 to January 2022. Two MLC1 WT cases were omitted from the final MWF analysis because of motion-related image artifacts.

MRI Acquisitions and Postprocessing

Imaging was conducted on a 3T MR system (Vida, Siemens Healthineers, Erlangen, Germany). A 6-channel birdcage coil (Stark Contrast, Erlangen, Germany) was employed for the animal scans. Three-dimensional MRF using stack-of-star trajectory was acquired with these settings: repetition time 10 ms; echo time 4.84 ms; field of view 60 × 60 × 24 mm³; voxel size 0.5 × 0.5 × 2 mm³; flip angle following sinusoidal variation; 640 MRF time points; 32 radial spokes per time point; slice-direction acceleration factor 3 (total scan duration: 17 min 55 sec) **(Figure 1).** Anatomical T2-weighted turbo spin echo images were obtained with: repetition time 3000 ms; echo time 64 ms; flip angle 150 degrees; field of view 42 × 42 mm²; resolution 0.1 × 0.1 mm²; slice thickness 1 mm; 18 slices; GRAPPA factor 2; 8 averages (scan time: 7 min 17 s).

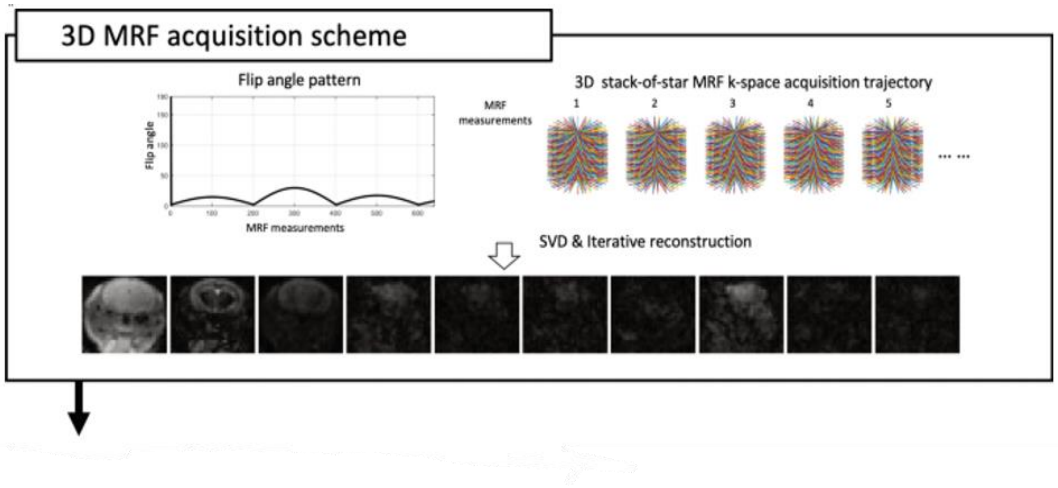

a)

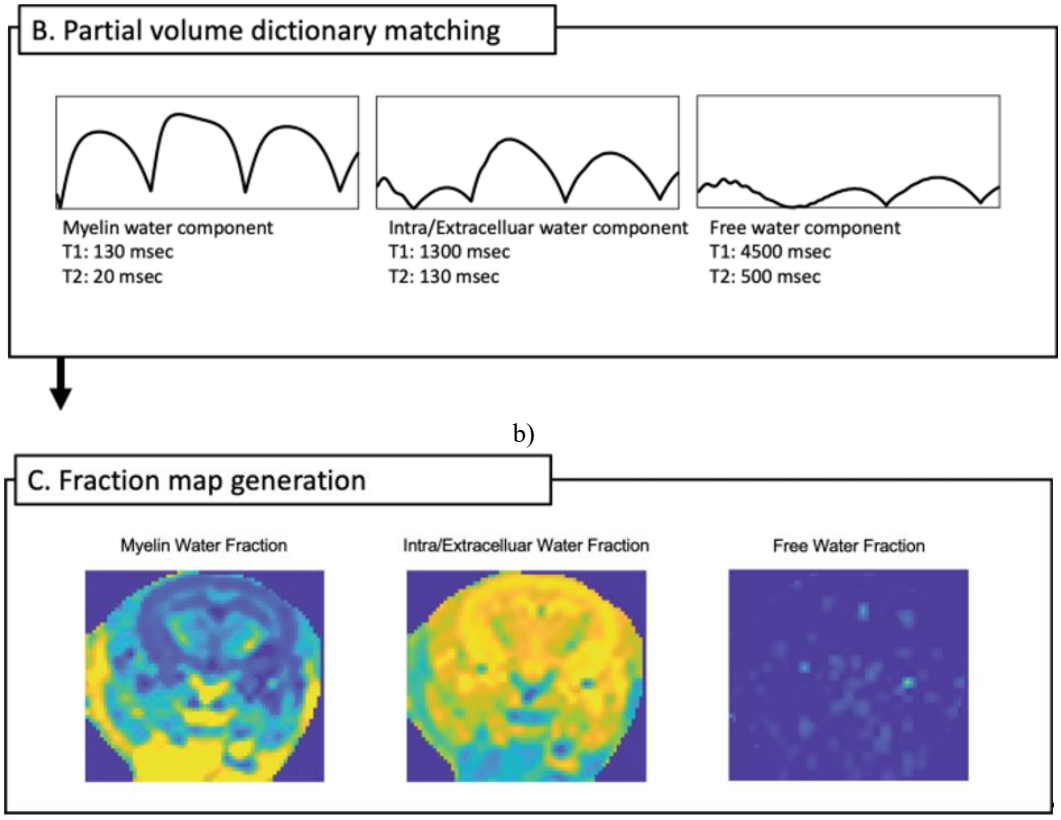

Figure 1. Overview of myelin water fraction (MWF) map creation via 3D magnetic resonance fingerprinting (MRF). Illustration of the 3D MRF scheme, reconstructed images with sinusoidal flip angle variation, and 3D stack-of-star trajectory (a). Signal curves for partial volume dictionary entries of each compartment (myelin, intra/extracellular, and free water) (b). Example fraction maps from a mouse following dictionary matching (c). SVD, singular value decomposition

T1 and T2 maps were generated from the 3D MRF data [2]. A three-compartment partial volume MRF approach from prior work [1] was then used to calculate MWF. Fixed relaxation values per compartment were: myelin water T1=130 ms, T2=20 ms; intra/extracellular water T1=1300 ms, T2=130 ms; free water T1=4500 ms, T2=500 ms **(Figure 1)** [1, 4]. Iterative reconstruction was applied to enhance image quality [2, 17]. The 3D MRF sequence relied on fast imaging with steady-state precession without radiofrequency spoilers or gradient spoiling. Sequence specifics and validation of T1/T2 accuracy from 3D MRF are detailed elsewhere [2, 17].

To examine MWF sensitivity to varied predefined myelin water T1 and T2 values, five alternative combinations were tested on one 13-month-old MLC1 WT and one 13-month-old MLC1 KO mouse: combination 1, T1=10 ms, T2=10 ms; combination 2, T1=65 ms, T2=20 ms; combination 3, T1=130 ms, T2=10 ms; combination 4, T1=252 ms, T2=15 ms; combination 5, T1=828 ms, T2=72 ms. Values for the other compartments remained fixed.

Immunohistochemistry

Brain sections from mice were stained using a mouse anti-proteolipid protein (PLP) antibody. Quantification of staining intensity was performed with NIH ImageJ software.

Data analysis

A board-certified radiologist (H.G.K., 14 years in pediatric neuroradiology) manually placed regions of interest in the corpus callosum and cortex on MWF maps, guided by each mouse's T2-weighted images, using ITK-SNAP (version 3.8.0; http://www.itksnap.org/). For immunohistochemical sections, a researcher (K.C., 19 years in mouse brain research) delineated corresponding

regions in the corpus callosum and cortex via NIH ImageJ.

Children study

Children

This retrospective pediatric analysis was approved by the Institutional Review Board, with waiver of informed consent. Three-dimensional MRF is incorporated into standard clinical brain MRI protocols at our center. Neonates undergo a feed-and-wrap approach with a MedVac infant immobilizer (CFI Medical, USA) for scanning [18]. Clinical MRI reports from June 2020 to June 2022 were screened sequentially, identifying 750 studies. Cases with any pathological findings, psychiatric conditions, or prematurity history were removed. Further exclusion of MRF acquisitions lacking B1 mapping left 81 studies for inclusion **(Figure 2)**.

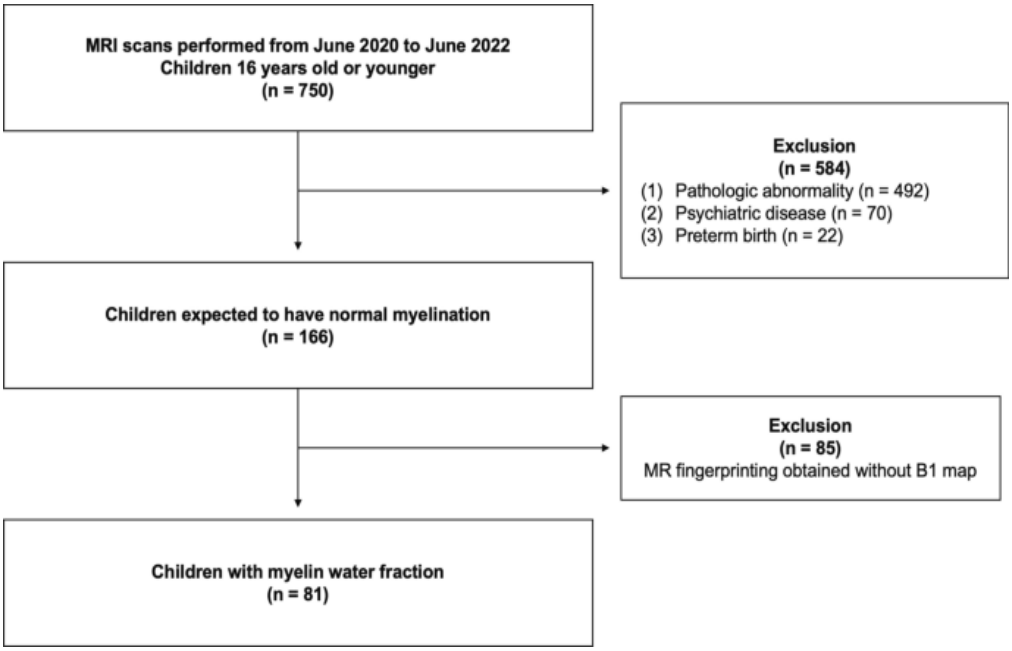

Figure 2. Diagram illustrating the selection process for pediatric participants

Cases were grouped by age: those ≤5 years and those >5 years. A board-certified pediatric radiologist (H.G.K., 14 years of expertise) reviewed all MRI scans and verified normal myelination patterns.

MRI acquisitions and postprocessing

Pediatric imaging employed a 64-channel head and neck coil. Three-dimensional MRF using hybrid radial-EPI trajectory [2] was acquired with these parameters: repetition time 7.7 ms; echo time 4.84 ms; field of view 256 × 256 × 144 mm^3; voxel size 0.7 × 0.7 × 2 mm^3; flip angle sinusoidal variation; 640 MRF time points; 6 radial spokes per time point; slice acceleration factor 5; echo train length in slice direction 4 (duration: 4 min 54 sec). T1, T2, and MWF maps were produced from 3D MRF data following the method outlined earlier [1, 2].

Data analysis

Regions of interest were manually placed by a board-certified radiologist (H.G.K., 14 years in pediatric neuroradiology) across frontal white matter, parietal white matter, occipital white matter, posterior limb of internal capsule, genu of corpus callosum, splenium of corpus callosum, caudate nucleus, putamen, and thalamus. Outlining was done on T1 maps for reference via ITK-SNAP (version 3.8.0; http://www.itksnap.org/).

Intra- and interobserver agreement

Intraobserver reliability for pediatric MWF was tested by having one board-certified radiologist (H.G.K., 14 years in pediatric neuroradiology) repeat region placement after two weeks. Interobserver reliability involved two blinded board-certified radiologists (J.K. and H.G.K., with 10 and 14 years in neuroradiology/pediatric neuroradiology) independently delineating regions.

Age-matched animals and children

To contrast MWF in the corpus callosum and cortex at equivalent developmental points, 3-week-old C57BL/6 mice and 12-year-old children were compared [19]. The genu of the corpus callosum was used as the target area in children.

Statistics

The Kolmogorov–Smirnov test checked normality. Mann–Whitney and Fisher's exact tests compared age and sex in MLC1 WT versus KO groups. Linear regression tested links between MWF and PLP-stained regions, and between MWF and age, in C57BL/6 mice by area (corpus callosum, cortex). For 12-week C57BL/6 mice, linear regression evaluated MWF versus pooled PLP from both areas. Mann–Whitney test contrasted MWF between MLC1 WT and KO; unpaired t-test contrasted PLP areas. In children, age-MWF patterns were visualized with scatter plots and fitted to nonlinear (second- or third-order) models, then compared. Age-T1 and age-T2 patterns used scatter plots with third-order fits. β values reflected weekly (mice) or yearly (children) shifts in MWF or PLP (%). Intraclass correlation coefficients (ICCs) measured reliability [20], with 0.61–0.80 indicating strong and 0.81–1.00 near-perfect agreement [21]. ICCs used mean-rating (k=2), absolute-agreement, two-way mixed model. Analyses ran on SPSS version 29 (SPSS) or GraphPad Prism version 8.4.2 (GraphPad), conducted by H.G.K. (14 years experience). Bonferroni correction applied; $P < 0.05$ is significant.

Results and Discussion

Characteristics of the study sample

Thirty-five C57BL/6 mice at varied ages (median 12 weeks; range 3–48 weeks) were analyzed: 3 weeks — 8 mice (6 females); 8 weeks — 8 mice (4 males); 12 weeks — 7 mice (4 males); 24 weeks — 5 mice (3 females); 48 weeks — 7 mice (4 males). For leukodystrophy contrasts, 9 MLC1 WT (median 17 months; range 12–20 months; 7 males) and 9 MLC1 KO (median 13 months; range 13–24 months; 6 females) were included. MWF evaluation used 9 MLC1 KO and 7 MLC1 WT (median 17 months; range 12–20 months; 6 males). Details on mouse groups appear in **Table 1.**

Table 1. Characteristics of the mice

Characteristic	MLC1 KO (n = 9)	MLC1 WT (n = 9)	C57BL/6 (n = 35)	MLC1 WT vs MLC1 KO *P* value
Age (weeks)	52 [24] (52–96)	68 [20] (48–80)	12 [16] (3–48)	0.80
Age (months)	13 [6] (13–24)	17 [5] (12–20)	3 [4] (1–12)	0.80
Sex				0.08
Male	3 (33)	7 (78)	16 (46)	
Female	6 (67)	2 (22)	19 (54)	

Data are displayed as medians accompanied by interquartile ranges in brackets and full ranges in parentheses, or as counts followed by percentages in parentheses

MLC1 = megalencephalic leukoencephalopathy with subcortical cyst 1, WT = wild type, KO = knock-out

Correlations with tissue myelin markers and developmental progression

In the complete set of C57BL/6 mice, MWF exhibited clear positive correlations with PLP-stained regions in the corpus callosum ($\beta = 0.0006$, $P = 0.04$) and cortex ($\beta = 0.0005$, $P = 0.006$) **(Figure 3a)**. Within the subset of 12-week-old C57BL/6 animals, MWF demonstrated a notable positive link to PLP staining ($\beta = 0.0009$, $P = 0.003$, $R^2 = 0.54$) **(Figure 3a).** Median MWF [IQR] across C57BL/6 mice was 0.1 [0.06] for corpus callosum and 0.08 [0.02] for cortex. Age displayed strong positive ties to MWF in the corpus callosum ($\beta = 0.0022$, $P < 0.001$) and cortex ($\beta = 0.0010$, $P < 0.001$) **(Figure 3b).** Typical examples of MWF maps paired with PLP staining from C57BL/6 mice across age groups are presented in **Figure 3c**.

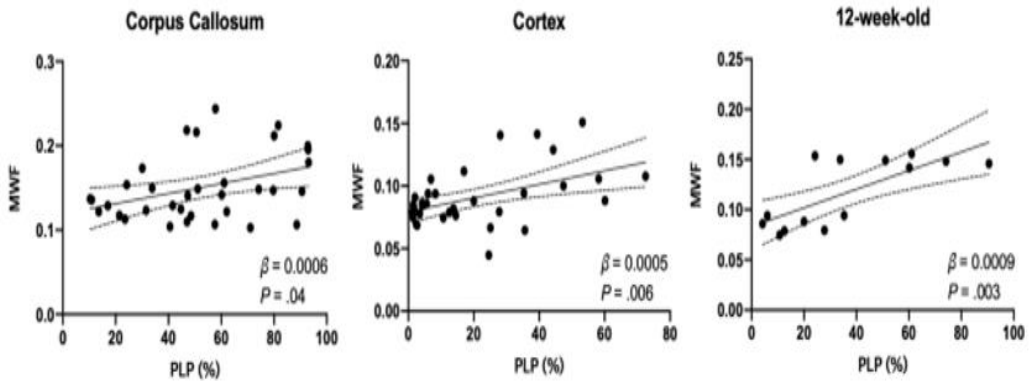

a)

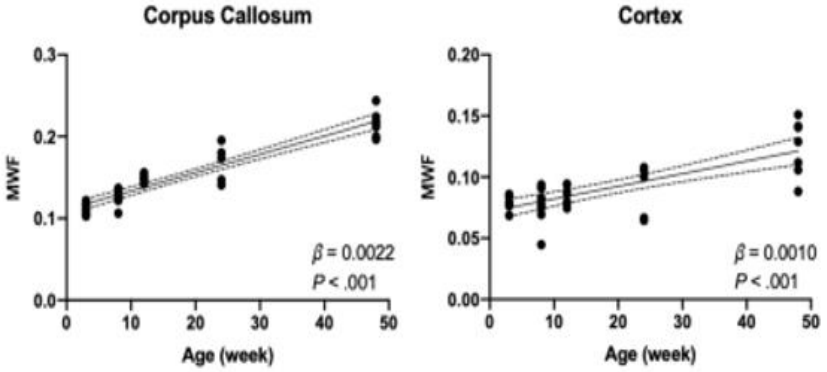

b)

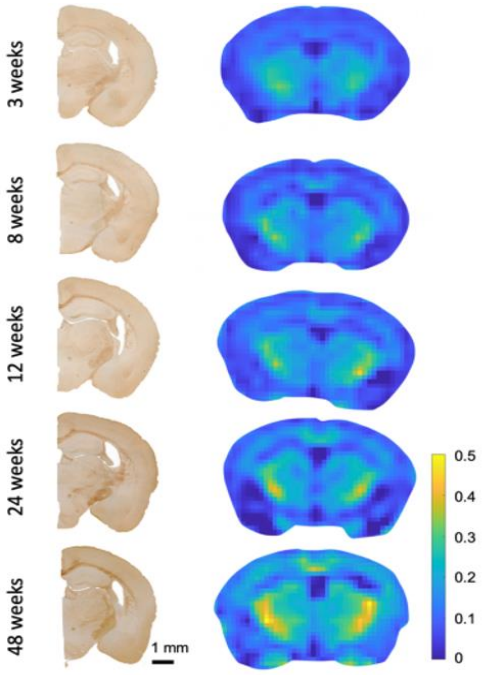

c)

Figure 3. Patterns of myelin water fraction (MWF) relative to proteolipid protein (PLP) staining levels and age progression. Robust links appeared between MWF and PLP intensity in corpus callosum (a, left) and cortex (a, middle) for the full C57BL/6 cohort, plus the seven 12-week-old cases (a, right). Age correlated markedly with

MWF rises in the corpus callosum (b, left) and cortex (b, right). Illustrative PLP-stained images (left) alongside corresponding MWF maps (right) from C57BL/6 mice at varying ages (c). Solid lines show optimal regression fits; dashed lines denote 95% confidence boundaries

Relations to hereditary white matter pathology in mouse models

MWF contrasts highlighted reductions in KO compared to WT mice in corpus callosum (0.20 [IQR, 0.03] vs 0.13 [IQR, 0.04]; P < 0.001) and cortex (0.12 [IQR, 0.02] vs 0.06 [IQR, 0.03]; P < 0.001**) (Table 2 and Figure 4a).** PLP staining intensity varied between WT and KO in corpus callosum (57% [IQR, 50%] vs 31% [IQR, 22%]; P = 0.03) yet showed no significant difference in cortex (86% [IQR, 74%] vs 42% [IQR, 62%]; P = 0.16) **(Table 2 and Figure 4b).** Sample MWF maps for MLC1 WT and KO cases are illustrated in **Figure 4c**.

Table 2. Contrasts between megalencephalic leukoencephalopathy subcortical cyst 1 wild-type and knock-out models

Parameter	MLC1 KO	MLC1 WT	*P* value
Myelin water fraction			
Corpus callosum	0.13 [0.04]	0.20 [0.03]	< 0.001
Cortex	0.06 [0.03]	0.12 [0.02]	< 0.001
PLP (%)			
Corpus callosum	31 [22]	57 [50]	0.03
Cortex	42 [62]	86 [74]	0.16

Data appear as medians with interquartile ranges in brackets and ranges in parentheses, or as mouse counts with percentages in parentheses
MLC1 = megalencephalic leukoencephalopathy with subcortical cyst 1, WT = wild type, KO = knock-out, PLP = anti-proteolipid protein immunoreactive area

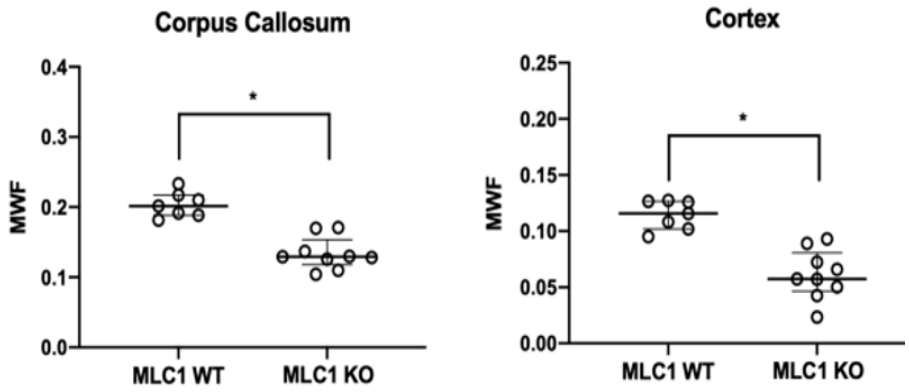

a)

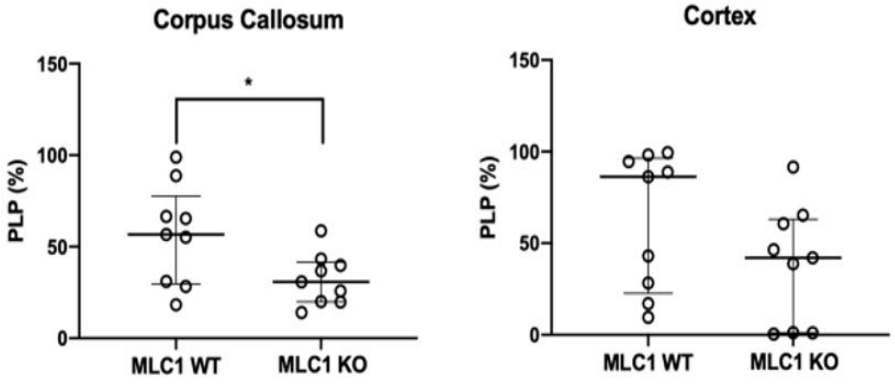

b)

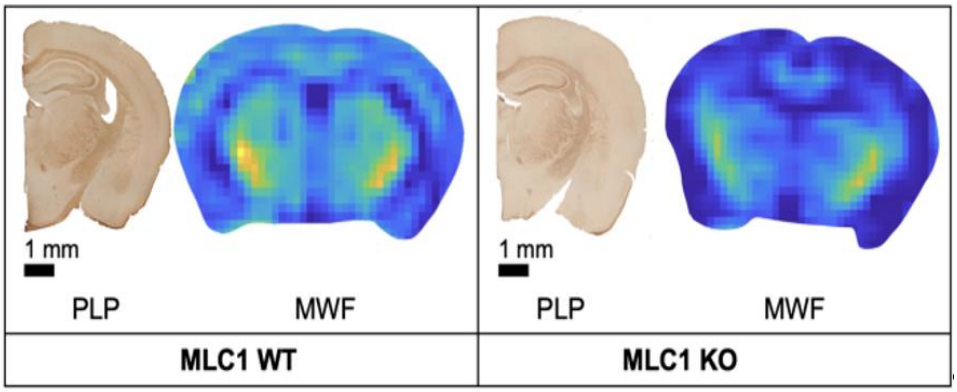

c)

Figure 4. Differences in myelin water fraction (MWF) and proteolipid protein (PLP) staining across control and disease-model mice. Lower MWF emerged in both the corpus callosum and cortex for MLC1 KO versus WT (a). PLP intensity reductions reached significance in the corpus callosum but not the cortex between groups (b). Typical PLP staining and MWF maps from 13-month-old MLC1 WT and KO animals (c). An asterisk (*) marks $P < 0.05$

MWF variations based on selected T1 and T2 settings

Table 3 outlines MWF results obtained using multiple preset T1 and T2 pairs for myelin water. Patterns remained stable regardless of the pair chosen: corpus callosum consistently yielded higher MWF than cortex, and MLC1 WT animals exceeded MLC1 KO animals. Specifically, Combination 1 (T1 and T2 both at 10 ms) produced lower MWF than the baseline pair. Combination 2, which raised T1 above baseline, led to decreased MWF. Conversely, Combination 3, featuring reduced T2, generated elevated MWF relative to baseline. Combinations 4 and 5, both with elevated T1 but contrasting T2 (lower in 4, higher in 5), resulted in higher MWF than the baseline.

Table 3. Myelin water fraction readings in megalencephalic leukoencephalopathy with subcortical cysts 1 wild-type and knock-out mice across different predefined myelin water T1 and T2 settings

Simulation	T1 (ms)	T2 (ms)	MLC1 KO mouse*		MLC1 WT mouse*	
			Corpus callosum	Cortex	Corpus callosum	Cortex
Original	130	20	0.121	0.021	0.178	0.123
1	10	10	0.008	0	0.022	0.006
2	65	20	0.058	0.001	0.101	0.057
3	130	10	0.159	0.037	0.221	0.158
4	252	15	0.243	0.130	0.312	0.256
5	828	72	0.837	0.574	0.888	0.837

* A 13-month-old mouse, MLC1 = megalencephalic leukoencephalopathy with subcortical cyst 1, WT = wild type, KO = knock-out

Children study

Participant profile

The cohort comprised 81 children (median age 126 months; range 0–199 months; 50 females). Among them, 57 were above 5 years (median age 151 months; range 68–199 months; 37 females). Participant details appear in **Table 4.**

Table 4. Characteristics of the children

Characteristic	Children (n = 81)
Age (months)	126 [144] (0–199)
Sex	
Male	31 (38)
Female	50 (62)

Data appear as medians with interquartile ranges in brackets and ranges in parentheses, or counts with percentages in parentheses

Age-related patterns in pediatric cases

Across all children, median MWF across brain areas spanned 0.03 to 0.44. For those ≤5 years, medians ranged 0–0.02; for those >5 years, 0.03–0.49. Scatter plots revealed clear age-dependent MWF increases across regions **(Figure 5a).** Both second- and third-order

regressions confirmed age-MWF links per region **(Table 5)**. Third-order models provided optimal fits (adjusted R^2 0.44–0.94, $P < 0.001$). Model comparisons favored third-order fits for frontal WM, parietal WM, occipital WM, posterior limb of internal capsule, genu of corpus callosum, and splenium of corpus callosum (P range <0.001–0.04). Example MWF maps from children at varying ages are displayed in **Figure 5b**. Regional T1 and T2 followed third-order age trajectories (T1 adjusted R^2 0.75−0.82, $P < 0.001$; T2 adjusted R^2 0.60−0.76, $P < 0.001$).

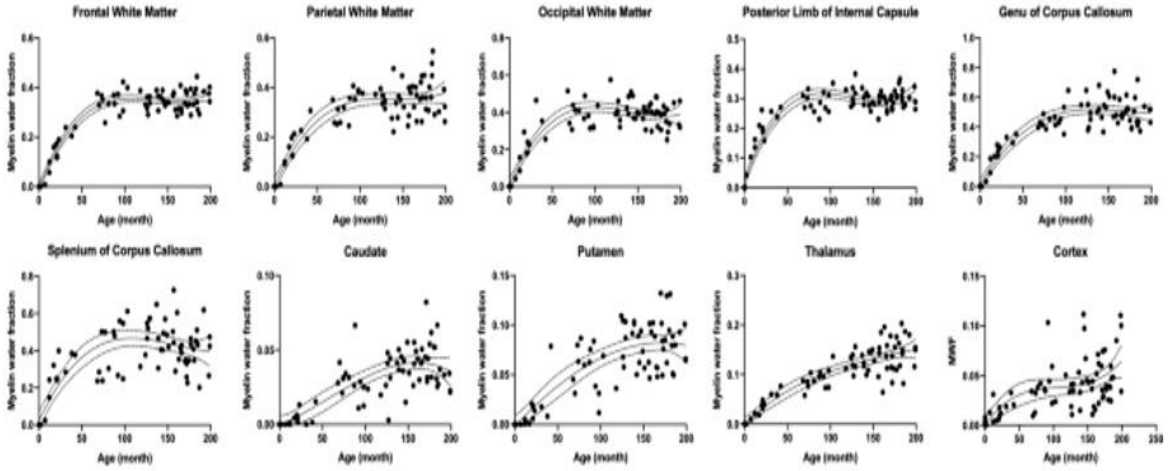

a)

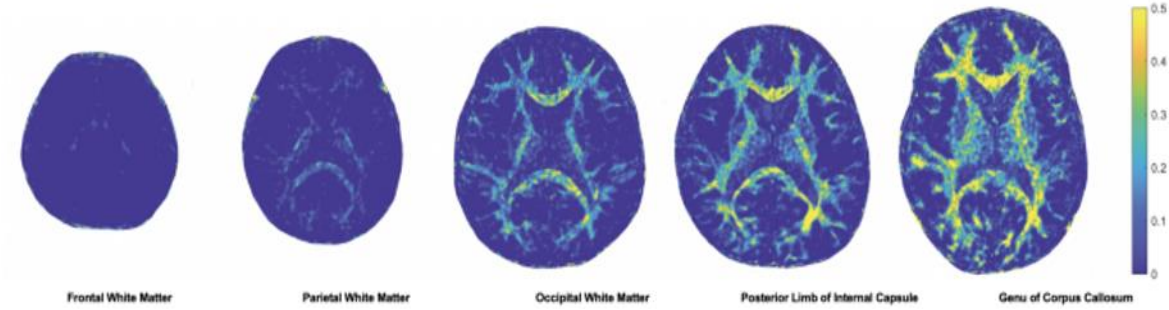

b)

Figure 5. Age-dependent myelin water fraction trends in pediatric subjects. Scatter plots depicting myelin water fraction across various brain areas versus age (a). Sample axial MR fingerprinting-based myelin water fraction maps from children at progressive ages (left to right: 2-month-old female, 7-month-old female, 20-month-old male, 42-month-old male, 161-month-old male) (b). Solid lines represent best-fit third-order regression; dashed lines mark 95% confidence bands

Table 5. Evaluation of regression models examining age-myelin water fraction associations.

Brain Region	Second-Order Regression			Third-Order Regression			Second- vs Third-Order Regression
	Adjusted R^2	RMSE	P value	Adjusted R^2	RMSE	P value	P value
Frontal white matter	0.90	0.04	< 0.001	0.94	0.03	< 0.001	< 0.001
Parietal white matter	0.83	0.06	< 0.001	0.85	0.06	< 0.001	0.002
Occipital white matter	0.81	0.07	< 0.001	0.84	0.06	< 0.001	< 0.001

Posterior limb of the internal capsule	0.83	0.05	< 0.001	0.90	0.03	< 0.001	< 0.001
Genu of the corpus callosum	0.86	0.08	< 0.001	0.86	0.08	< 0.001	0.04
Splenium of the corpus callosum	0.68	0.11	< 0.001	0.69	0.10	< 0.001	< 0.001
Caudate	0.64	0.01	< 0.001	0.65	0.01	< 0.001	0.19
Putamen	0.70	0.02	< 0.001	0.70	0.02	< 0.001	0.88
Thalamus	0.83	0.02	< 0.001	0.83	0.02	< 0.001	0.39
Cortex	0.42	0.02	< 0.001	0.44	0.02	< 0.001	0.06

RMSE = root mean squared error

Reliability across observers

Intraobserver reliability for MWF ranged from strong to nearly perfect, with ICC values between 0.71 (95% CI: 0.55, 0.81) and 0.99 (95% CI: 0.99, 0.99) across brain areas. Interobserver reliability similarly spanned strong to near-perfect, with ICC from 0.71 (95% CI: 0.55, 0.81) to 0.95 (95% CI: 0.92, 0.97).

Developmentally matched mouse and human comparisons

The group included 8 C57BL/6 mice aged 3 weeks and 5 children aged 12 years. Median [IQR] MWF in the corpus callosum reached 0.11 [0.01] for the young mice and 0.53 [0.15] for the children. Cortical median [IQR] MWF was 0.08 [0.01] in the 3-week mice and 0.05 [0.03] in the 12-year-old children.

Quantifying myelin through brain MRI plays a key role in monitoring typical maturation and detecting leukodystrophies. Although MWF serves as a valuable myelin marker, MRF-based MWF lacked prior tissue validation and large-scale testing. Here, we examined untreated mice across ages and transgenic leukodystrophy models. In both corpus callosum and cortex, 3D MRF MWF correlated positively with histological myelin staining and rose with age. Leukodystrophy-model mice displayed reduced MWF relative to controls. Across 81 typically developing children, MWF followed expected maturation trajectories, best captured by third-order regression fits.

We conducted tissue-based validation of 3D MRF MWF in age-varied mice and leukodystrophy models. Such validation is crucial prior to broader preclinical or clinical adoption. Previous reports linked MWF from animals and humans to demyelination [22, 23] or autism [24, 25]. MWF can stem from T2, T2*, T1, or steady-state sequences [5]. Unlike those, 3D MRF delivers rapid, high-resolution whole-brain scans under 10 min [2]. Our approach used a hybrid radial-interleaved EPI 3D MRF. Earlier work validated 2D synthetic MRI (QRAPMASTER multi-echo saturation recovery) histologically against Luxol fast blue, yielding Spearman $r = 0.74$ and $R^2 = 0.55$ [26]. Our MRF MWF versus PLP showed comparable linear regression ($\beta = 0.0009$, $R^2 = 0.54$). That study reported mean myelin 0.31 (white matter) and 0.05 (gray matter) [26], aligning with our older children (median frontal WM 0.35, putamen 0.08). Direct cross-study comparisons remain limited, as MRI myelin signals explain only ~54–55% of true density variance, with methods differing (PLP here vs Luxol fast blue there). Various myelin stains (Luxol fast blue, PLP, myelin basic protein, myelin oligodendrocyte glycoprotein) can diverge in demyelination/remyelination contexts despite overall myelination reflection [27]. Identifying optimal marker-MRI pairings for specific scenarios warrants further exploration. Thus, our mouse validation supports the 3D MRF MWF promise, though methodological differences constrain direct benchmarking and call for more research.

Age-driven MWF increases emerged in both mice and children, consistent with prior reports [28, 29]. We demonstrated 3D MRF MWF utility for quantitative maturation tracking. Traditionally, maturation relied on qualitative spatial patterns, but quantitative [2, 6] and automated [30] tools now prevail. Myelin dynamics across pediatric and adult ages feature widely [1, 2, 6, 29, 31]. Pediatric in vivo myelin metrics often fit nonlinear curves [6, 32]. Our results mirrored known myelination trajectories, though lower cortical/subcortical MWF (0.03–0.10) raises accuracy concerns—cortex thinness risks partial volume effects, and 3D MRF resolution may limit precision. Still, given demonstrated abnormalities in autism [24, 25] or prematurity [33, 34], relative maturation grading via 3D MRF holds clinical value.

Beyond MRF and synthetic MRI, numerous MRI approaches exist for estimating myelin content, such as ultra-short echo-time (UTE), magnetization transfer (MT), inhomogeneous magnetization transfer (ihMT), and quantitative susceptibility mapping (QSM) [35]. Of these, ihMT and QSM have achieved exceptionally high correlations with myelin in preclinical models (R^2 = 0.85−0.94), while UTE and MT displayed robust correlations (R^2 = 0.51−0.60) [35]. Our findings revealed a comparable robust correlation for MWF against PLP staining (R^2 = 0.54), matching earlier MWF investigations (R^2 = 0.55) [35]. Unlike ihMT and QSM, which serve as indirect myelin-mapping techniques, MRF represents a swift, direct multiparametric quantitative method that generates parameter maps straight from acquired signals [36]. MRF efficiently produces T1, T2, and MWF maps in shorter times, in contrast to indirect techniques that demand longer acquisitions and yield fewer parameters. Considering the critical need for brief scans in infants, MRF was selected here. Nonetheless, emerging methods like ihMT and QSM will likely supplement precise myelin evaluation in future work.

In this investigation, MLC1 KO mice (leukodystrophy model) exhibited reduced MWF compared to MLC1 WT controls, a pattern that held across multiple preset myelin water T1 and T2 pairs. MLC represents a hereditary condition marked by cerebral white matter swelling [37]. Tissue analysis reveals expanded brain volume and vacuoles within myelin sheaths in MLC [37]. Such changes appear in mice as young as 3 months and intensify by 7–12 months [38]. Our myelin assessment in MLC mice detected significant cortical MWF reductions between KO and WT, alongside a downward trend in PLP staining for KO. Since both MWF and PLP in the corpus callosum indicated clear declines from MLC1 knockout, MWF might detect leukodystrophy-related shifts more readily, though validation requires larger cohorts across ages. Furthermore, given links between MLC genetic variants and clinical outcomes [39], MWF could aid in subclassifying genotypes.

Developmentally aligned comparisons showed parallel MWF patterns in corpus callosum (mice 0.11; children 0.53) and cortex (mice 0.08; children 0.05) between species. Cross-species MRI myelin research remains limited, likely due to challenges in harmonizing protocols. Mouse imaging typically uses ultra-high-field systems (≥7 T), while human scans employ clinical fields (≤3 T). One report tracked myelin progression in dogs and monkeys via T2 relaxation on a 2.35 T scanner [40], hinting at interspecies potential, though without direct quantitative cross-comparisons—possibly emphasizing maturation stage over species traits.

Several constraints apply to this work. First, MWF derivation relied on a three-compartment model from earlier reports [1, 4], using adult- and child-derived preset T1/T2 values [1, 4]. Resulting MWF exceeded some previous estimates [41], and sensitivity testing confirmed influence from these presets **(Table 3).** Upcoming efforts should derive compartment-specific relaxation values optimized for age groups. Applicability of identical modeling across mice and humans also merits scrutiny. Second, the mismatched age spans between the mouse (up to 48 weeks, roughly 38–47 human years [19]) and pediatric (up to 16 years) cohorts hinder precise cross-species developmental matching. Extending the algorithm to adult humans could prove valuable. Third, retrospective pediatric data may include subtle myelination influencers despite exclusions for overt pathology or risk histories; full normalcy cannot be guaranteed. Fourth, motion susceptibility in young children risks artifactual MWF alteration. Neonates benefited from feed-and-wrap immobilization, but older cases lacked dedicated mitigation beyond routine sedation where used. Motion elimination proves difficult, yet prior evidence suggests MRF resilience [42]. Dedicated motion impact studies on MRF-derived MWF are advisable.

Conclusion

Overall, 3D MRF yielded MWF across age-varying mice, leukodystrophy models, and pediatric subjects. These MWF readings closely matched histopathological myelin markers. Age-related MWF elevations emerged in both species. Leukodystrophy mice displayed diminished MWF versus controls. Thus, 3D MRF-based MWF emerges as a viable, quick, non-invasive myelin biomarker applicable to mice and humans. Refining compartment T1/T2 settings for each species remains essential for diagnostic reliability. Prospective longitudinal tracking of typical and disordered maturation via MWF could solidify its utility for prognosis and therapy monitoring in affected individuals.

Acknowledgments: None

Conflict of Interest: None

Financial Support: None

Ethics Statement: None

References

1. Chen Y, Chen MH, Baluyot KR, Potts TM, Jimenez J, Lin W, et al. MR fingerprinting enables quantitative measures of brain tissue relaxation times and myelin water fraction in the first five years of life. Neuroimage. 2019;186:782–793. doi: 10.1016/j.neuroimage.2018.11.038
2. Yu N, Kim JY, Han D, Kim SY, Lee HM, Kim DH, et al. Three-dimensional magnetic resonance fingerprinting in neonates: quantifying regional difference and maturation in the brain. Invest Radiol. 2022;57:44–51. doi: 10.1097/RLI.0000000000000800
3. Ma D, Gulani V, Seiberlich N, Liu K, Sunshine JL, Duerk JL, et al. Magnetic resonance fingerprinting. Nature. 2013;495:187–192. doi: 10.1038/nature11971
4. Deshmane A, Badve C, Rogers M, Yu A, Ma D, Sunshine J, et al. Tissue Mapping in Brain Tumors with Partial Volume Magnetic Resonance Fingerprinting (PV-MRF). 23rd Annual Meeting and Exhibition of the International Society for Magnetic Resonance in Medicine (ISMRM 2015); 2015.
5. Lee J, Hyun JW, Lee J, Choi EJ, Shin HG, Min K, et al. So you want to image myelin using mri: an overview and practical guide for myelin water imaging. J Magn Reson Imaging. 2021;53:360–373. doi: 10.1002/jmri.27059
6. Kim HG, Moon WJ, Han J, Choi JW. Quantification of myelin in children using multiparametric quantitative MRI: a pilot study. Neuroradiology. 2017;59:1043–1051. doi: 10.1007/s00234-017-1889-9
7. Sternberger NH, Quarles RH, Itoyama Y, Webster HD. Myelin-associated glycoprotein demonstrated immunocytochemically in myelin and myelin-forming cells of developing rat. Proc Natl Acad Sci U S A. 1979;76:1510–1514. doi: 10.1073/pnas.76.3.1510
8. Barkovich AJ. Concepts of myelin and myelination in neuroradiology. AJNR Am J Neuroradiol. 2000;21:1099–1109.
9. Engelbrecht V, Scherer A, Rassek M, Witsack HJ, Modder U. Diffusion-weighted MR imaging in the brain in children: findings in the normal brain and in the brain with white matter diseases. Radiology. 2002;222:410–418. doi: 10.1148/radiol.2222010492
10. Bonkowsky JL, Nelson C, Kingston JL, Filloux FM, Mundorff MB, Srivastava R. The burden of inherited leukodystrophies in children. Neurology. 2010;75:718–725. doi: 10.1212/WNL.0b013e3181eee46b
11. Cheon JE, Kim IO, Hwang YS, Kim KJ, Wang KC, Cho BK, et al. Leukodystrophy in children: a pictorial review of MR imaging features. Radiographics. 2002;22:461–476. doi: 10.1148/radiographics.22.3.g02ma01461
12. Ridder MC, Boor I, Lodder JC, Postma NL, Capdevila-Nortes X, Duarri A, et al. Megalencephalic leucoencephalopathy with cysts: defect in chloride currents and cell volume regulation. Brain. 2011;134:3342–3354. doi: 10.1093/brain/awr255
13. van der Knaap MS, Barth PG, Stroink H, van Nieuwenhuizen O, Arts WF, Hoogenraad F, et al. Leukoencephalopathy with swelling and a discrepantly mild clinical course in eight children. Ann Neurol. 1995;37:324–334. doi: 10.1002/ana.410370308
14. van der Voorn JP, Pouwels PJ, Hart AA, Serrarens J, Willemsen MA, Kremer HP, et al. Childhood white matter disorders: quantitative MR imaging and spectroscopy. Radiology. 2006;241:510–517. doi: 10.1148/radiol.2412051345
15. Duarri A, Teijido O, Lopez-Hernandez T, Scheper GC, Barriere H, Boor I, et al. Molecular pathogenesis of megalencephalic leukoencephalopathy with subcortical cysts: mutations in MLC1 cause folding defects. Hum Mol Genet. 2008;17:3728–3739. doi: 10.1093/hmg/ddn269
16. Brockmann K, Finsterbusch J, Terwey B, Frahm J, Hanefeld F. Megalencephalic leukoencephalopathy with subcortical cysts in an adult: quantitative proton MR spectroscopy and diffusion tensor MRI. Neuroradiology. 2003;45:137–142. doi: 10.1007/s00234-002-0931-7
17. Han D, Hong T, Lee Y, Kim D-H. High Resolution 3D magnetic resonance fingerprinting with hybrid radial-interleaved EPI acquisition for knee cartilage T1, T2 mapping. Investigative Magnetic Resonance

Imaging. 2021;25:141–155. doi: 10.13104/imri.2021.25.3.141
18. Yu NL, Lee HM, Kim HG, Kim S-Y. The Success of Brain Magnetic Resonance Imaging in Non-Sedated Infants. Perinatology. 2022;33:136–142. doi: 10.14734/PN.2022.33.3.136
19. Flurkey K, Currer JM, Harrison D. Mouse models in aging research. The mouse in biomedical research. New York: Elsevier; 2007. pp. 637–672.
20. Fleiss JL, Levin B, Paik MC. The measurement of interrater agreement. Statist Methods Rates Proportions. 1981;2:22–23.
21. Landis JR, Koch GG. The measurement of observer agreement for categorical data. Biometrics. 1977;33:159–174. doi: 10.2307/2529310
22. Soustelle L, Antal MC, Lamy J, Rousseau F, Armspach JP, LoureirodeSousa P. Correlations of quantitative MRI metrics with myelin basic protein (MBP) staining in a murine model of demyelination. NMR Biomed. 2019;32:4116. doi: 10.1002/nbm.4116
23. Laule C, Vavasour IM, Moore GR, Oger J, Li DK, Paty DW, et al. Water content and myelin water fraction in multiple sclerosis A T2 relaxation study. J Neurol. 2004;251:284–293. doi: 10.1007/s00415-004-0306-6
24. Khanbabaei M, Hughes E, Ellegood J, Qiu LR, Yip R, Dobry J, et al. Precocious myelination in a mouse model of autism. Transl Psychiatry. 2019;9:251. doi: 10.1038/s41398-019-0590-7
25. Deoni SC, Zinkstok JR, Daly E, Ecker C, Consortiuma MA, Williams SC, et al. White-matter relaxation time and myelin water fraction differences in young adults with autism. Psychol Med. 2015;45:795–805.
26. Warntjes JBM, Persson A, Berge J, Zech W. Myelin detection using rapid quantitative MR imaging correlated to macroscopically registered luxol fast blue-stained brain specimens. AJNR Am J Neuroradiol. 2017;38:1096–1102. doi: 10.3174/ajnr.A5168
27. Lindner M, Heine S, Haastert K, Garde N, Fokuhl J, Linsmeier F, et al. Sequential myelin protein expression during remyelination reveals fast and efficient repair after central nervous system demyelination. Neuropathol Appl Neurobiol. 2008;34:105–114. doi: 10.1111/j.1365-2990.2007.00879.x
28. Hammelrath L, Skokic S, Khmelinskii A, Hess A, van der Knaap N, Staring M, et al. Morphological maturation of the mouse brain: An in vivo MRI and histology investigation. Neuroimage. 2016;125:144–152. doi: 10.1016/j.neuroimage.2015.10.009
29. Lebel C, Treit S, Beaulieu C. A review of diffusion MRI of typical white matter development from early childhood to young adulthood. NMR Biomed. 2019;32:e3778. doi: 10.1002/nbm.3778
30. Chen JV, Chaudhari G, Hess CP, Glenn OA, Sugrue LP, Rauschecker AM, et al. Deep learning to predict neonatal and infant brain age from myelination on brain MRI Scans. Radiology. 2022;305:678–687. doi: 10.1148/radiol.211860
31. Faizy TD, Kumar D, Broocks G, Thaler C, Flottmann F, Leischner H, et al. Age-Related Measurements of the Myelin Water Fraction derived from 3D multi-echo GRASE reflect Myelin Content of the Cerebral White Matter. Sci Rep. 2018;8:14991. doi: 10.1038/s41598-018-33112-8
32. Lee SM, Choi YH, You S-K, Lee WK, Kim WH, Kim HJ, et al. Age-related changes in tissue value properties in children: simultaneous quantification of relaxation times and proton density using synthetic magnetic resonance imaging. Invest Radiol. 2018;53:236–245. doi: 10.1097/RLI.0000000000000435
33. Vandewouw MM, Young JM, Shroff MM, Taylor MJ, Sled JG. Altered myelin maturation in four year old children born very preterm. Neuroimage Clin. 2019;21:101635. doi: 10.1016/j.nicl.2018.101635
34. McNaughton R, Pieper C, Sakai O, Rollins JV, Zhang X, Kennedy DN, et al. Quantitative MRI characterization of the extremely preterm brain at adolescence: atypical versus neurotypical developmental pathways. Radiology. 2022;304:419–428. doi: 10.1148/radiol.210385
35. van der Weijden CWJ, Biondetti E, Gutmann IW, Dijkstra H, McKerchar R, de Paula FD, et al. Quantitative myelin imaging with MRI and PET: an overview of techniques and their validation status. Brain. 2023;146:1243–1266. doi: 10.1093/brain/awac436
36. Jara H, Sakai O, Farrher E, Oros-Peusquens AM, Shah NJ, Alsop DC, et al. Primary multiparametric quantitative brain MRI: state-of-the-art relaxometric and proton density mapping techniques. Radiology. 2022;305:5–18. doi: 10.1148/radiol.211519

37. van der Knaap MS, Boor I, Estevez R. Megalencephalic leukoencephalopathy with subcortical cysts: chronic white matter oedema due to a defect in brain ion and water homoeostasis. Lancet Neurol. 2012;11:973–985. doi: 10.1016/S1474-4422(12)70192-8
38. Dubey M, Bugiani M, Ridder MC, Postma NL, Brouwers E, Polder E, et al. Mice with megalencephalic leukoencephalopathy with cysts: a developmental angle. Ann Neurol. 2015;77:114–131. doi: 10.1002/ana.24307
39. Hamilton EMC, Tekturk P, Cialdella F, van Rappard DF, Wolf NI, Yalcinkaya C, et al. Megalencephalic leukoencephalopathy with subcortical cysts: Characterization of disease variants. Neurology. 2018;90:e1395–e1403. doi: 10.1212/WNL.0000000000005334
40. Miot-Noirault E, Barantin L, Akoka S, Le Pape A. T2 relaxation time as a marker of brain myelination: experimental MR study in two neonatal animal models. J Neurosci Methods. 1997;72:5–14. doi: 10.1016/S0165-0270(96)00148-3
41. MacKay AL, Laule C. Magnetic Resonance of Myelin Water: An in vivo Marker for Myelin. Brain Plast. 2016;2:71–91. doi: 10.3233/BPL-160033
42. Ma D, Badve C, Sun JEP, Hu S, Wang X, Chen Y, et al. Motion Robust MR Fingerprinting Scan to Image Neonates With Prenatal Opioid Exposure. J Magn Reson Imaging. 2023;56:4. doi: 10.1002/jmri.28907